ALMA reveals the aftermath of a white dwarf–brown dwarf merger in CK Vulpeculae

S. P. S. Eyres[1,2], A. Evans[3], A. Zijlstra[4], A. Avison[4], R. D. Gehrz[5], M. Hajduk[6], S. Starrfield[7], S. Mohamed[8], C. E. Woodward[5], R. M. Wagner[9,10]

[1]*Faculty of Computing, Engineering & Science, University of South Wales, Pontypridd CF37 1DL, UK*
[2]*Jeremiah Horrocks Institute, University of Central Lancashire, Preston PR1 2HE, UK*
[3]*Astrophysics Group, Keele University, Keele, Staffordshire ST5 5BG, UK*
[4]*Jodrell Bank Centre for Astrophysics, School of Physics and Astronomy, University of Manchester, Manchester, M13 9PL, UK*
[5]*Minnesota Institute for Astrophysics, School of Physics & Astronomy, 116 Church Street SE, University of Minnesota, Minneapolis, MN 55455, USA*
[6]*Space Radio-Diagnostics Research Centre, University of Warmia and Mazury, Prawochenskiego Str. 9, 10-720 Olsztyn, Poland*
[7]*School of Earth and Space Exploration, Arizona State University, Box 871404, Tempe, AZ 85287-1404, USA*
[8]*South African Astronomical Observatory, PO Box 9, Observatory 7935, Cape Town, Western Cape, South Africa*
[9]*Department of Astronomy, The Ohio State University, 140 West 18th Avenue, Columbus, OH 43210, USA*
[10]*LBT Observatory, University of Arizona, Tucson, AZ 85721-0065, USA*

ABSTRACT

We present Atacama Large Millimeter–Submillimeter Array (ALMA) observations of CK Vulpeculae which is identified with "Nova Vulpeculae 1670". They trace obscuring dust in the inner regions of the associated nebulosity. The dust forms two cocoons, each extending $\sim 5''$ north and south of the presumed location of the central star. Brighter emission is in a more compact east–west structure ($2'' \times 1''$) where the cocoons intersect. We detect line emission in NH_2CHO, CN, four organic molecules and $C^{17}O$. CN lines trace bubbles within the dusty cocoons; CH_3OH a north–south S–shaped jet; and other molecules a central cloud with a structure aligned with the innermost dust structure. The major axis of the overall dust and gas bubble structure has a projected inclination of $\sim 24°$ with respect to a $71''$ extended "hourglass" nebulosity, previously seen in Hα. Three cocoon limbs align with dark lanes in the inner regions of the same Hα images. The central $2'' \times 1''$ dust is resolved into a structure consistent with a warped dusty disc. The velocity structure of the jets indicates an origin at the centre of this disc and precession with an unknown period. Deceleration regions at both the northern and southern tips of the jets are roughly coincident with additional diffuse dust emission over regions approximately $2''$ across. These structures are consistent with a bipolar outflow expanding into surrounding high density material. We suggest that a white dwarf and brown dwarf merged between 1670 and 1672, with the observed structures and extraordinary isotopic abundances generated as a result.

Key words: circumstellar matter – stars: individual, CK Vul – stars: peculiar – stars: jets – stars: winds, outflows – Submillimetre: stars

1 INTRODUCTION

Nova Vul 1670 was discovered at 3rd magnitude by Père Dom Anthelme on 20 June 1670, and is described in contemporary accounts as *Nova sub Capite Cygni* (see for example Figure 1 of Shara, Moffat & Webbink 1985). Using Hα imaging, Shara & Moffat (1982) claimed to have recov-

ered the remnant of the 1670 event[1] and had it proven to have been a classical nova, the object might have provided a means of investigating the inter–outburst behaviour of this class. In a detailed study, Shara et al. (1985) reconstructed the original observations of Nova Vul 1670 in the form of a light curve calibrated to the modern magnitude scale, showing two peaks brighter than 3rd magnitude in 1670 and 1671.

---

[1] We refer to the 1670 event as "Nova Vul 1670" and to the object observed post–1980 as CK Vul.

However Shara et al. (1985) recognised that there are serious shortcomings with this interpretation. For example the light curve is extremely un–nova–like, and the expansion velocity implied by the current size of the remnant is implausibly slow, even for a very slow classical nova. They and others have considered several alternative interpretations, which have (over time) included a Herbig–Haro object, a late thermal pulse, a "diffusion–induced nova", and a stellar merger (see Evans et al. 2016; Kamiński et al. 2015, 2017, for discussion).

Hajduk et al. (2007) found a radio source at the position of CK Vul. They interpreted this as optically thin free–free emission, implying that the central source must be hot enough to ionise the nebula; on the assumption that the radio emission is free–free, they estimate a mass of $4 \times 10^{-7}\,\mathrm{M_\odot}$ for the ionised gas. They also discovered a faint extended bipolar ($\sim 71''$) Hα nebula, presenting evidence that it is expanding, with an origin – centred on the radio source – consistent with a 1670 ejection event. They speculated that the radio source could be associated with a circumbinary disc, similar to those seen in some binary post–AGB stars.

Evans et al. (2016) presented *Spitzer* IRS spectroscopy in the range 5.8–40.0 μm. They found emission from HCN, H$_2$, [O IV], [Si II] and [Si III], together with Unidentified Infrared (UIR) emission – consistent with dust formed in a carbon–rich environment. Excitation of the UIR features requires a source of ultraviolet radiation; the central wavelength of the '7.7 μm' and '11.2 μm' UIR features imply an effective temperature of at least $\sim$14 000 K.

From the arguments in Evans et al. (2016) regarding the UIR features and the presence of ionised species such as [O IV], the Hα emission, and the free–free radio source (Hajduk et al. 2007), there is a considerable amount of evidence to suggest that there is a source of ultraviolet radiation at the heart of CK Vul.

Kamiński et al. (2015) observed CK Vul with the Atacama Pathfinder Experiment (APEX; Güsten et al. 2004), and found a rich spectrum of diatomic and triatomic molecules; they used isotopologues to estimate the ^{12}C/^{13}C, ^{14}N/^{15}N and ^{16}O/^{18}O isotopic ratios, all of which are grossly non–solar (and non–nova). These isotope ratios suggest non–equilibrium CNO burning, possibly at an elevated temperature. Kamiński et al. also observed CK Vul with the Submillimeter Array (SMA; Ho et al. 2002), finding both a jet structure in CO(3–2) emission with an extent of $13''$ north–south, and dust emission arising from the same region as the radio emission detected by Hajduk et al. (2007). The dust source has structure $\sim 3.7'' \times \sim 1.0''$ at PA 33°, but there is other structure as well. They suggested that the dust emission arises in a torus/disc and a pair of jets.

Further observations with APEX and IRAM (Kamiński et al. 2017) extend the spectroscopy over a range from $\sim$70 to $\sim$900 GHz, with spatial resolution at frequency ν of $8073''/\nu$ (APEX) and $3393''/\nu$ (IRAM), or between $\sim 9''$ and $\sim 48''$ (900 down to 70 GHz). They identify emission from 27 molecules, comprising the elements H, C, N, O, F, Al, Si, P, and S.

Here we present high spatial resolution imaging of the dust emission from the inner $\sim 24''$ of the system, taken with the Atacama Large Millimeter–Submillimeter Array (ALMA; Wootten & Thompson 2009). We examine the dust emission as well as line emission from gas in a range of structures, extending north and south of the central source approximately $5''$ in each direction.

2   OBSERVATIONS

Observations were made of CK Vul with ALMA at Band 6, in four spectral windows 1.875 GHz in width and centred on 224 GHz, 226 GHz, 240 GHz and 242 GHz. These are referred to as SPW0, SPW1, SPW2 and SPW3 respectively for brevity. Data were collected in 128 channels in each window, giving a modest velocity resolution slightly better than 21 km s^{-1}. Channels 0–7 and 119–127 (SPW0 and SPW1), and channels 0–8 and 120–127 (SPW2 and SPW3), sit outside the system bandpass.

Our selected sensitivity and spatial resolution targets were met with two observations: 10 min 8 sec in array configuration C40–3; and 23 min 18 sec in an intermediate array of approximately the same antenna distribution as array configuration C40–6. The latter data are referred to as the C40–6 data for brevity, although in practice the longest baseline exceeded that of the standard configuration.

The C40–3 data were taken starting at 2017 April 24 11:47:53 UT, using J2148+0657 as flux calibrator (see van Kempen et al. 2015, for a discussion of ALMA calibrators), J2025+3343 as bandpass calibrator and J1935+2031 as phase calibrator. The array incorporated 39 antennae, with a maximum baseline of 460 m and minimum baseline of 15.1 m.

The C40–6 data were taken starting at 2017 July 22 03:26:07 UT, using J1751+0939 as flux and bandpass calibrators, and J1952+2526 as phase calibrator. The array incorporated 42 antennae, with a maximum baseline of 3.7 km and minimum baseline of 16.7 m.

The data were recovered from the ALMA archive and calibrated using the standard scripts provided by the pipeline. The two sets of calibrated data were then combined into a single *uv* measurement set using CASA task concat(McMullin et al. 2007), with default settings except copypointing=False as we are not mosaicing.

By inspection of the calibrated amplitude versus frequency in each spectral window, as provided by the calibration pipeline, we identified the following channels as containing continuum emission: SPW0 25 to 118; SPW1 50 to 75 and 90 to 118; SPW2 all; and SPW3 9 to 35 and 95 to 119.

The continuum channels were used to derive a map of the dust emission, using CASA task tclean. Briggs weighting was applied with robust=2. The resultant image has a beam of 280 milliarcsec by 250 milliarcsec, with the major axis at position angle $-177°$.

These channel ranges were then used to remove the continuum data in the *uv* plane, using uvcontsub. The continuum–subtracted data in each spectral window were then imaged in spectral cube mode to allow examination of the emission. The spatial resolution varies slightly across the channels in the four spectral windows, but is close enough to the continuum resolution to be considered identical for the purposes of comparison. We detect eight distinct lines showing extended emission. We have identified these lines as outlined in Table 1, and show an integrated spectrum in Fig 1.

A spectral cube was extracted for each line across all
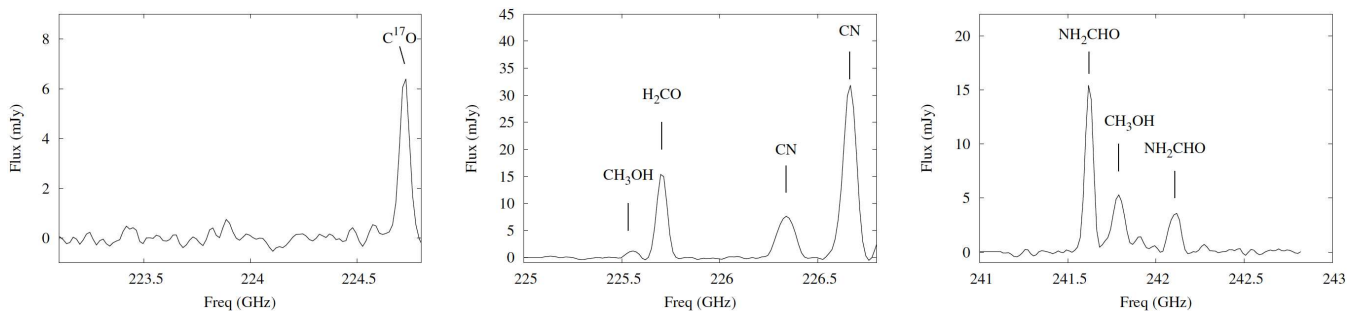
Figure 1. Integrated spectra indicating the eight lines listed in Table 1. Note the additional line rising at the edge of the band just above the strong CN line at 226.66 GHz; this line contributes to the high velocity emission depicted in Fig 3(d).

Table 1. Line identifications.

Line	Observed central frequency (GHz)	Rest frequency[*] (GHz)	Line identification
1	224.273 ± 0.001	224.695	$C^{17}O$
2	225.553 ± 0.003	225.524	CH_3OH
3	225.704 ± 0.001	225.675	H_2CO
4	226.338 ± 0.001	226.309	CN
5	226.663 ± 0.001	226.634	CN
6	241.621 ± 0.001	241.590	NH_2CHO
7	241.787 ± 0.001	241.756	CH_3OH
8	242.107 ± 0.001	242.076	NH_2CHO

[*]Assuming $v_{LSR} = -38 \, \text{km s}^{-1}$ calculated for 2017 April 24.

channels showing emission from that line. The frequency of the fitted peak for the corresponding line (given in Table 1) was then assigned the $v_{LSR} = -38 \, \text{km s}^{-1}$, obtained using the Starlink rv package (Wallace & Clayton 1997; Currie et al. 2014). The frequency of each line differs from the v_{LSR}–adjusted frequency by less than the spectral resolution, except for the line at observed frequency[2] 225.553 GHz (CH_3OH, but see below for a discussion of the emission distribution for this line). This allows us to understand the velocity structure in comparison to the local standard of rest. For the cube containing the 226.663 GHz line (see Table 1), structure at the edge of the band is associated with an adjacent line centred beyond the edge of the spectral window at 226.85 GHz, as can be seen at the edge of the middle panel of Fig 1. The rest frequency for that feature differs from the value assigned to that cube, and is unknown as the centre is not in the band.

We defer modelling of the dynamics of these emission lines to a future, more detailed, paper; for our present purposes we confine the discussion to a comparison of the distribution of selected lines with the dust emission.

3 RESULTS

Kamiński et al. (2015) associate the continuum emission around 230 GHz with dust, based on the spectral energy distribution (SED). They report a central distribution extended north–south and east–west. Taken together this allows us to associate the continuum emission in Fig. 2(a) with

the dust distribution, the central peak being aligned with the point of origin for the expansion discussed by Hajduk et al. (2007). The axis of the north–south extension is consistent with that of the CO jet identified by Kamiński et al. (2015).

3.1 The dust

Determination of the dust mass (see Section 3.1.2 below) requires the distance to CK Vul. For consistency with most of the work on this object, we adopt a value of $D = 700$ pc throughout (Hajduk et al. 2013; Kamiński et al. 2015). We also assume a continuum observing wavelength of 1249 μm, which at 240.2 GHz sits in SWP2 and is representative for the continuum.

3.1.1 The dust distribution

There are three distinct components to the dust distribution (see Fig 2(a)):

(i) Four "arcs" of emission that extend $4''$ to $6''$, two each to the north and south, and which in three cases align well with dark lanes in the Hα emission reported by Hajduk et al. (2007) (see Fig. 2(b)).
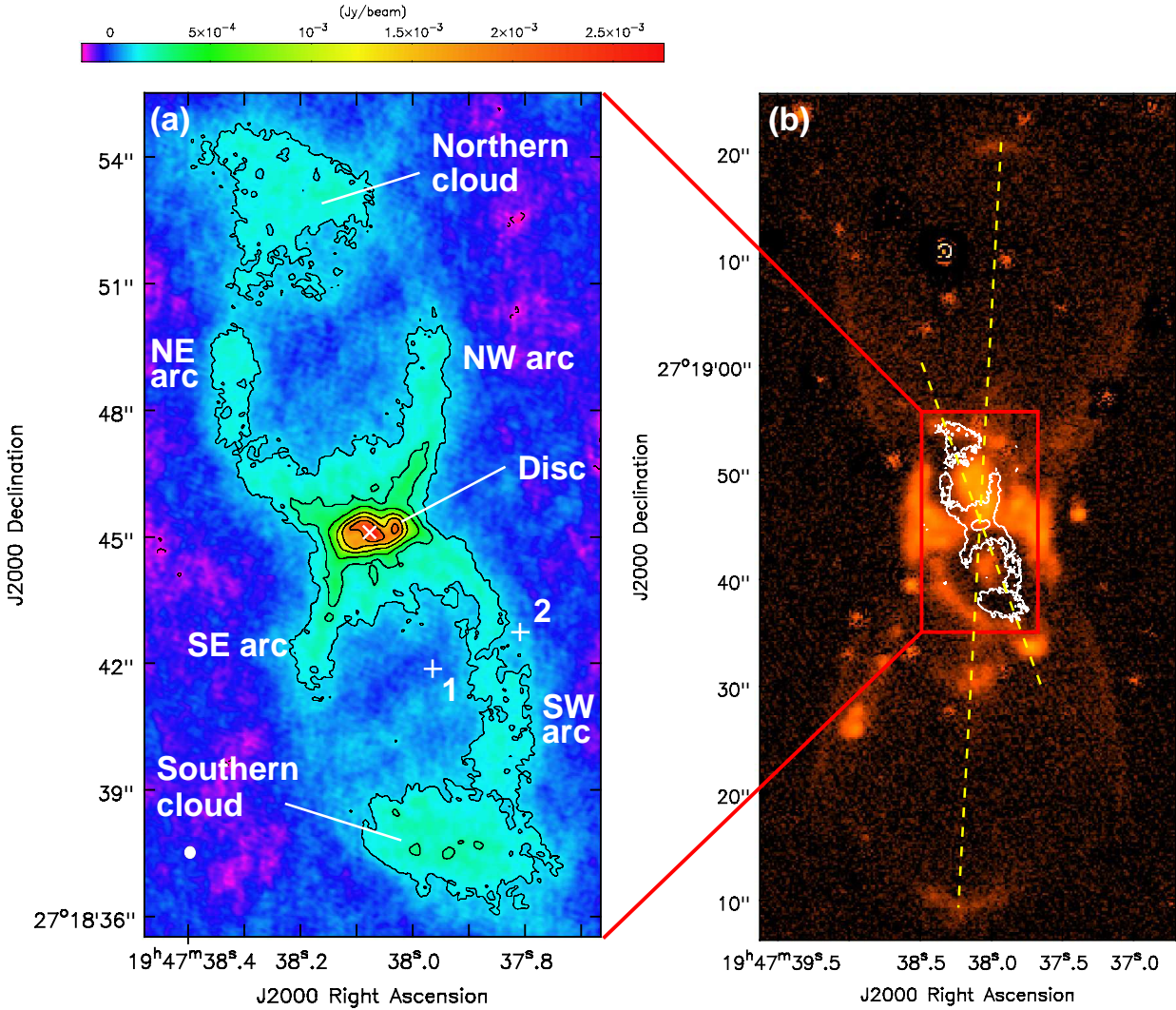
(ii) Some $6''$ to both north and south, there are faint, irregular but elongated regions ("clouds") approximately $3'' \times 4''$. The "major axes" of these features are oriented NE–SW, and are approximately orthogonal to the NE and SW arcs at the point the arcs appear to intersect with the clouds.

(iii) The inner $\sim 2''$ is extended east–west with a substructure that includes north–south extension around the peak, suggestive of a warped disc. We refer to this as the compact region, to differentiate from the diffuse emission in the arcs and clouds. The free–free radio source reported by Hajduk et al. (2007) coincides with the brightest part of this feature within the errors, and the peak position of this is marked with an X in Fig. 2(a).

The dust emission has approximate point symmetry about the position of the radio source, and hence the putative stellar remnant. The central component resembles a warped disc, commonly seen in protoplanetary discs, where they may be the result of irradiation (e.g. Nixon & Pringle 2010) or the presence of massive planetary bodies (e.g. Walsh et al. 2017).

The major axes of diffuse dust emission (the arcs and

---

[2] All frequencies in the discussion that follows are the observed frequencies in Table 1.

Figure 2. Dust emission from CK Vul as observed by ALMA. (a) continuum emission associated with dust, contours at −0.12, 0.12, 0.24, 0.48, 0.96, 1.44 and 1.92 mJy beam^{-1}. The colour scale descends to 3σ and shows the emission between the arcs to north and south. Spatial resolution is represented by the small white circle in the bottom left of the image. The peak of the free–free emission reported by Hajduk et ql. (2007) is marked with an X, the location of the two variable stars discussed in that paper and in Section 3.1 are marked with crosses, labelled 1 and 2. (b) Dust emission (contours at 0.12 and 0.48 mJy beam^{-1} for reference) in relation to the extended Hα emission (Hajduk et al. 2007). The white ring at 19:47:38.3 27:19:10 is a saturated star in the Hα image. Red solid lines are included to demonstrate the relative scales of the two imaged regions. Dashed yellow lines indicate the major axes of the dust and Hα emission referred to in the text.

clouds) and those of the Hα hourglass reported by Hajduk et al. (2007) are misaligned (see Fig. 2(b), in which we mark these two axes as dashed lines): the major axis of the dust lobes has position angle $\sim 13°$, whereas that of the tip of the Hα emission is $\sim 349°$. If these features are due to outflows of essentially the same nature, but ejected at different times and hence at different points in the evolution of the central object, there has been some precession in the intervening time, amounting to $\sim 24°$ projected on to the sky. This may be related to the warped disc, noted above. This is consistent with the interpretation of a similar misalignment as precession, by Kamiński et al. (2015)

The distribution of the dust in space, rather than that projected on the sky, can be characterised from the observed variation across the structure. If it is arranged in four narrow

"filaments", we would expect to see essentially no emission in between each pair of arcs. On the other hand if the dust is distributed in hourglass–like "cocoons", then optically thin emission from the arcs (of width ΔR) should be a factor $\sim \sqrt{2R/\Delta R + 1} \sim 2.3$ brighter than from between the arcs (separated by distance R). The latter is close to what is observed, suggesting the observed arcs are projections of these dust cocoons.

The two variable stars discussed by Hajduk et al. (2007), are marked on Fig. 2(a), at the positions in Table 2. The variability was attributed to a varying dust distribution in the foreground, and the proposed dust was associated with CK Vul. They further proposed that the lithium absorption in both stars arises from the ejecta from Nova Vul 1670. The ALMA observations place the eastern star (1) behind

Table 2. Positions (J2000) of two variable stars from Hajduk, van Hoof & Zijlstra (2013) and marked in Fig. 2.

Star	RA	Dec
1	19:47:37.964	+27:18:41.86
2	19:47:37.811	+27:18:42.74

the central cavity of the dust cocoon, while the western star (2) is at the western edge of the cocoon. Thus the interpretation by Hajduk et al. (2007) would seem consistent with the resolved dust structure. In R band, Hajduk et al. (2007) found star 1 to have brightened by around 1.5 mag between 1983 and 2010, while star 2 declined by around 2 mag between 1991 and 2010. This would indicate a reduction in the dust along the line of sight to star 1, and an increase along the line of sight to star 2. This would be consistent with the southern jet currently depositing dust along the line of sight towards star 2, while the dust in front of star 1 is dispersing now that the jet has precessed to a different position.

3.1.2 Dust mass and the gas–to–dust ratio

Due to the irregular distribution of the dust emission, we have estimated the flux density using a "pixel counting" method. For the inner region shown in Fig. 2(a) we added up the total flux included within the 0.48 mJy beam^{-1} contour; this included 2226 pixels and gave a total flux density of 31.31±0.04 mJy. For the entire dust emission, we added up the total flux included within the 0.12 mJy beam^{-1} contour, a region containing 61903 pixels, finding a value of 132.84±0.04 mJy. Estimates of uncertainty were made by calculating the rms brightness in regions containing no dust emission. We note this is higher than the value of 75.0±0.4 mJy measured by Kamiński et al. (2015), but we image the dust over a larger area. From the difference between the total dust emission and that in the inner region, we estimate that the emission from the diffuse regions alone amounts to 101.53±0.06 mJy.

Kamiński et al. (2015) have a dual grey body model for the CK Vul mm/sub–mm SED, with dust temperatures $T = 15$ K and $T = 49$ K. The IR–mm SED in these papers suggests that the ALMA emission lies on the Rayleigh–Jeans tail for both temperatures. Given the abundance of hydrocarbons in the environment of CK Vul (Evans et al. 2016; Kamiński et al. 2015), we use the mass absorption coefficient for amorphous carbon ("AC") from Mennella et al. (1995), who give a value 66 cm^2 g^{-1} at 1100 μm. Thus

$$\frac{M_{\rm dust}}{\rm M_\odot} \simeq 3.18 \times 10^{-5} \left(\frac{D}{\rm kpc}\right)^2 \left(\frac{f_\nu}{\rm mJy}\right) \left(\frac{T}{\rm K}\right)^{-1} \left(\frac{\lambda}{1100\,\mu\rm m}\right)^{2.9} \tag{1}$$

for the dust mass. The SED in Kamiński et al. shows the 15 K emission dominates at 230 GHz. Using this as the temperature of the dust in Fig. 2(a), we find a total mass of $M_{\rm dust} \sim 2.04 \times 10^{-4}\,{\rm M_\odot}$. Of this $\sim 1.56 \times 10^{-4}\,{\rm M_\odot}$ is in the diffuse extended emission, and $\sim 4.81 \times 10^{-5}\,{\rm M_\odot}$ is in the central disc.

Kamiński et al. (2015) quote a gas mass of $\sim 1\,{\rm M_\odot}$, which results in a gas–to–dust ratio $\sim 10^4$ by mass, a value that is 10–100 times that seen in similar nebulae (e.g. Sarkar

& Sahai 2007; Otsuka 2017; Walsh et al. 2016). Assuming the CO column density in Kamiński et al., and a CO/H$_2$ ratio of $\sim 10^{-3}$ (appropriate for carbon–rich AGB winds), we recalculated a H$_2$ mass of $\sim 9.8 \times 10^{-3}\,{\rm M_\odot}$. We note that while most of the species identified by Kamiński et al. (2017) are carbon bearing, there are also numerous oxygen bearing molecules in their list. If the nebula is considered oxygen–rich, this will give a value $\sim 3.9 \times 10^{-2}\,{\rm M_\odot}$.

These are likely to be a lower limit on the hydrogen mass as much of this may be in atomic and ionic form. But if we assume $M_{\rm gas} \sim 9.8 \times 10^{-3}$ to $3.9 \times 10^{-2}\,{\rm M_\odot}$, and using the total dust mass estimate from the ALMA observation, the gas–to–dust ratio is ~ 50 to 200, which seems more reasonable. Thus calculating the H$_2$ ratio in a manner consistent with the observed nature of the nebula leads to a mass estimate that is also consistent with the dust mass we determine. Kamiński et al. (2017) justifiably describe CK Vul as having an "extraordinary isotopic composition", which may imply any adopted typical CO/H$_2$ ratio could be misleading, but there is no basis for adopting the gas–to–gas ratio of $\sim 10^4$ required for a mass of 1 M$_\odot$. Thus a value of 0.01 to 0.1 M$_\odot$ would seem most plausible given the other derived mass estimates.

3.2 The lines

In order to examine the structures present in the lines in Table 1 we have taken velocity cuts along the extended features, which are generally aligned north–south, consistent with the dust distribution and the CO jet detected by Kamiński et al. (2015). We have collapsed the data cubes to show the spatial distribution of the emission. The CN line at 226.663 GHz and the CH$_3$OH line at 241.787 GHz show the clearest extended structure and are presented here (see Fig. 3, where the intensity maps show the integrated emission from the spectral data cubes, collapsed along the velocity axis).

The CH$_3$OH line at 241.787 GHz shows a triple structure in the collapsed map in Fig. 3(a), with bridges of emission between the northern, central and southern features, together forming an "S" shape. A position–velocity plot is included in Fig. 3(b). This runs from north to south along the direction of the dashed line, integrating emission across the 99–pixel wide region between the parallel solid lines. This is consistent with a jet of gas in a direction that makes a small angle to the plane of the sky, and either decelerates or is dramatically redirected as it arrives at the north and south features, implying that it is encountering a region of higher density. Comparison with the dust distribution shows that the NE–SW extension of the central CH$_3$OH peak is consistent with the direction of the inner–most dust emission (inner–most contour in Fig. 2(a)). The N and S features are located with the ends of the dust arcs just before emission from the clouds begins, i.e. on the border of these regions closest to the central structure. Kamiński et al. (2017) detect this line, with an identification as CH$_3$OH.

The 226.663 GHz CN line shows a structure that is well–aligned with the dusty arcs to the NW and SE of the central emission. To the NE the line emission sits to the west of the adjacent arc, while to SW it sits to the east of the adjacent arc (Fig. 3(c)). The latter two components are better aligned with the jet traced by CH$_3$OH (compare (Figs. 3(a) and
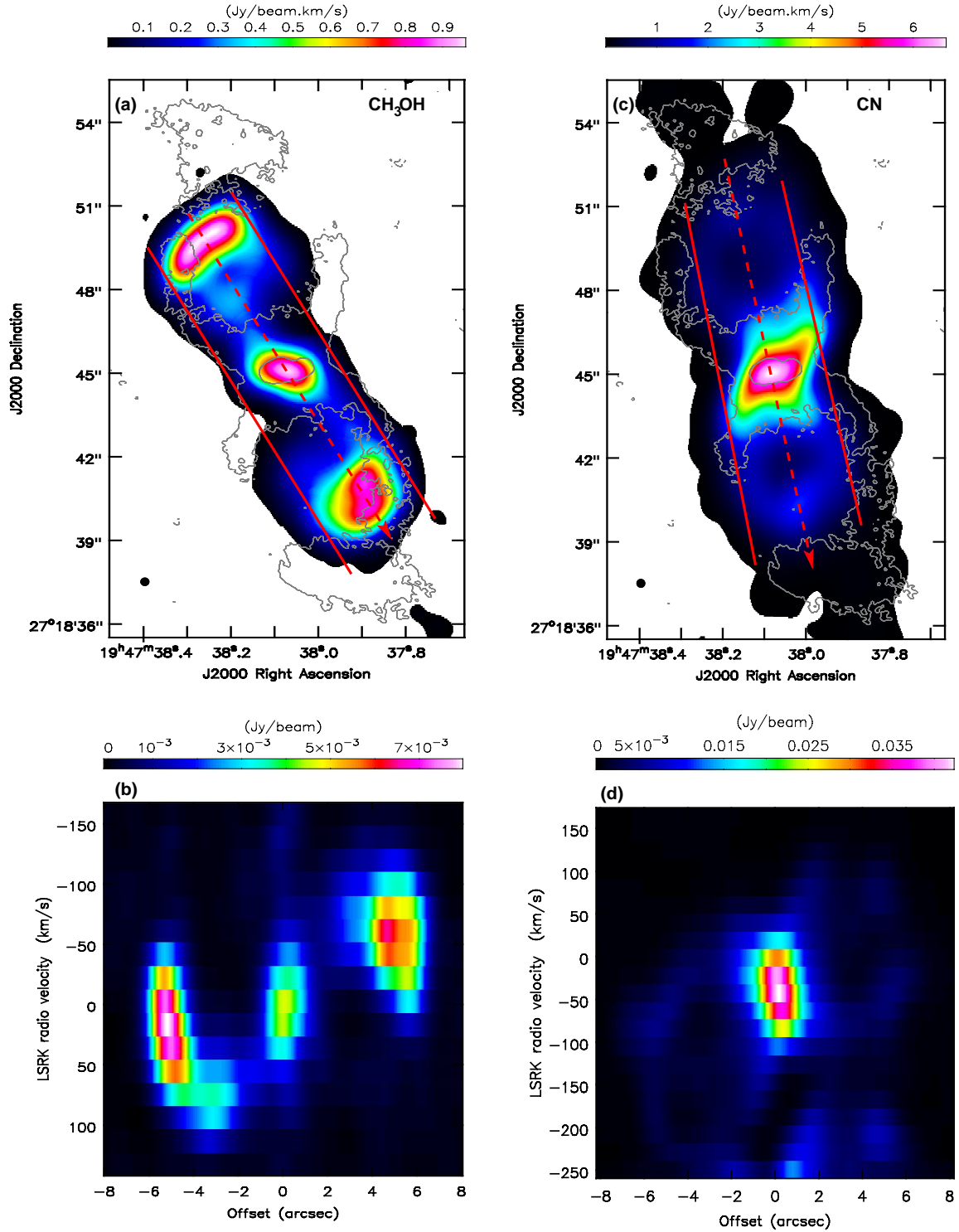
Figure 3. (a) Intensity map of the 241.787 GHz CH$_3$OH (colour scale, see Table 1); contours of dust continuum at 0.12 and 0.48 mJy beam^{-1} for reference; (b) position–velocity plot along the dashed–line with arrow in (a); (c) intensity map of the 226.663 GHz CN line (colour scale), contours as (a); (d) position–velocity plot along the dashed–line with arrow in (b) from north to south. For the intensity maps in (a) and (c) the spatial resolution is represented by the small black circle to the bottom left in each image, where both the spectral line and continuum resolutions are over–plotted, but are indistinguishable at this scale.
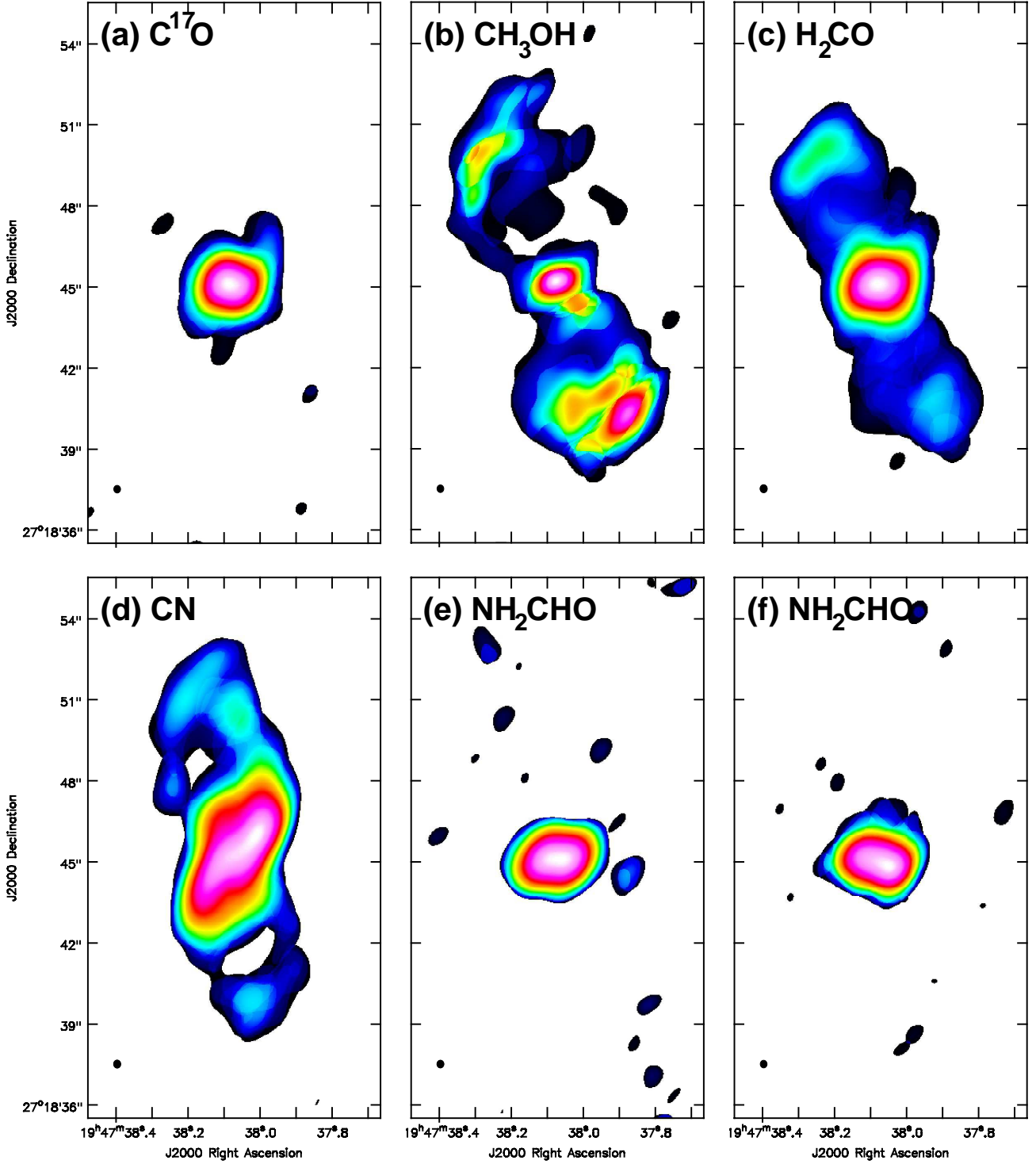
Figure 4. Intensity maps of (a) C^{17}O; (b) CH$_3$OH; (c) H$_2$CO; (d) CN; (e) NH$_2$CHO; (f) NH$_2$CHO. Colour scales are omitted for clarity; they differ in each case, but cover the full range of the brightness, refer to Fig. 1 for relative line strengths. The spatial resolution is represented by the small black circle to the bottom left in each image. Line numbers relate to those in Table 1.

(c)). Overall they form "loops" on the sky that trace the inner boundary of the dust structures. The velocity profile north to south in the direction of the dashed line in Fig 2(c) including the 99–pixel wide region between the parallel solid lines, is presented in Fig. 3(d). This also show loops, and is consistent with expanding bubbles. Taken together this suggests this gas is arranged in two bubbles expanding at $\sim 140\,\mathrm{km\,s^{-1}}$, traced north and south of the central feature. Kamiński et al. (2017) identified this line as CN, as well as the adjacent CN line with a peak that sits just outside SPW1. The 226.338 GHz line (also CN) shows a similar, but fainter structure.

Referring to Fig. 4, the lines at 224.273 ($\mathrm{C^{17}O}$), 241.621 GHz and 242.107 GHz both ($\mathrm{NH_2CHO}$) show only emission approximately coincident with the dust emission from the compact region (Fig. 2(a)); for the 241.621 GHz line this aligns with the overall dust distribution, but without the warped–disc substructure. The 225.553 GHz and 225.704 GHz lines are more difficult to disentangle, but overall appear to agree with the jet structure traced by the 241.787 GHz $\mathrm{CH_3OH}$ line; there are elements of the 226.663 GHz bubbles present also.

The line–of–sight velocity structures of the bubbles and the jets are consistent with the gaseous northern features being angled towards the Earth, with the southern features angled away, consistent with Hajduk et al. (2007). The orientation of the dust arcs is harder to constrain. The north–western one is overlaid with Hα emission. As we argue that we are seeing along the limb of a cocoon, the gas in the north angled towards the Earth is then not affected by local dust extinction, but that in the south and to the north–east sits behind the dusty hourglass.

4   DISCUSSION

Hajduk et al. (2007) argue that the extended, hour–glass Hα emitting material was ejected by Nova Vul 1670. We suggest that the dust condensed in material that was ejected more recently, after the central engine had precessed. Further, it seems clear that mass–loss is ongoing, as the jets and bubbles traced by molecular emission are consistent with outflows originating in the central engine. The shape of the jet is consistent with ongoing precession.

In addition we suggest that the coincidence of the dust arcs, which are due to long path lengths through the edges of the dusty cocoons, are causing the dark lanes in the Hα emission through extinction. It is difficult to see why H would be absent from only the points on the cocoons that happen to be the edges of those structures as they appear on the sky. If this was the case it would suggest either these regions have been cleared of Hydrogen (and presumably all other) gas or that the conditions do not support the excitation of the Balmer lines. We cannot rule this out.

The molecular gas, the dust and the gas traced by Hα in the inner region we believe all originate from activity after events of the 1670s.

The symmetry of the dust emission, the molecular line emission, and the Hα emission all strongly suggest that the central object is currently, or was in the past, a multiple system (see de Marco 2009, for a review).

4.1   Stellar mergers

We discard the possiblity that a stellar merger (see e.g. Kamiński et al. 2017, and references therein) between stars at the main sequence or giant phases of evolution can account for what is observed.

Hajduk et al. (2007) estimate the current luminosity of the central object to be $\sim 1 \pm 0.5\,\mathrm{L_\odot}$, based on the requirements to ionise the radio source they detect. Geometrical effects could push this to no more than a few times that value, certainly somewhat less than $10\,\mathrm{L_\odot}$. As a stellar merger event preserves the luminosity available to the pre–merger system in the post–merger system, this constrains the nature of the progenitor.

Bally & Zinnecker (2005) model a merger in a multiple stellar system. They expect an outburst luminosity $\sim 10^5 L_\odot$, and predict outflow velocities for typical parameters of a few times $30\,\mathrm{km\,s^{-1}}$. They also describe a debris disc with a size of around 1000 AU, and cooling timescales for the merged object between 1000 and 10 000 yr. Comparing the various characteristics of CK Vul with their predictions gives a picture consistent with the parameters from the Bally & Zinnecker modelling. However their work relates to the formation of high–mass stars through the merger of precursors with masses greater than 10 $\mathrm{M_\odot}$. Thus the luminosity estimate of Hajduk et al. (2007) excludes this as a possible model for CK Vul; our ejecta mass estimate of $0.1\,\mathrm{M_\odot}$ or lower is also consistent with a low–mass progenitor.

Metzger & Pejcha (2017) have modelled a group of stars including V838 Mon and V1309 Sco, with which CK Vul has been compared. They note that a double–peaked light curve (as was the case for Nova Vul 1670; Shara et al. 1985) is a common characteristic of these objects, and relate the time between light curve peaks t_{pk} (in days) to the physical characteristics of a stellar merger, which they propose as the origin of these systems. Rearranging their Equation (21), and substituting for the escape velocity to eliminate the pre–merger binary orbital radius, one finds the binary mass to be given by

$$\frac{M_{\mathrm{binary}}}{\mathrm{M_\odot}} \simeq \frac{t_{\mathrm{pk}}^2}{4.52 \times 10^6} \frac{\xi}{\kappa} \frac{v_{\mathrm{ej}}}{M_{\mathrm{ej}}} \qquad (2)$$

where M_{ej} is the ejecta mass in solar masses, v_{ej} the ejecta velocity in $\mathrm{km\,s^{-1}}$, and $\xi/\kappa \sim 2$ for reasonable values. For CK Vul we have estimated $M_{\mathrm{ej}} \sim 10^{-2}\,\mathrm{M_\odot}$. Hajduk et al. (2013) estimated $M_{\mathrm{ej}} \sim 5 \times 10^{-2}\,\mathrm{M_\odot}$ for a gas–to–dust ratio of 100. Ejecta velocities in the literature are in the range 60 to $200\,\mathrm{km\,s^{-1}}$; the time between peaks in 1670 and 1671 gives $t_{\mathrm{pk}} \sim 270$ d (estimated from the lightcurve in Shara et al. 1985, by comparing the dates of the two peaks). This gives $40 < M_{\mathrm{binary}} < 650\,\mathrm{M_\odot}$, a range excluded by the Hajduk et al. (2007) luminosity estimate. We note we have used the lower limit of our ejecta mass estimate.

We conclude that no stellar merger models for main sequence to giant star progenitors can account for the properties of CK Vul either during the 1670s events or in contemporary observations.

4.2   Planet ingestion

Retter & Marom (2003) invoked a red giant branch (RGB) star "swallowing" a number of planets to account for the 2003

outburst of the transient V838 Mon, with which CK Vul has been compared (Kato 2003). Soker & Tylenda (2007) outlined a number of fundamental reasons, including the energy and mass available in a planet, as to why the Retter & Marom model could not explain V838 Mon. Other modelling of planet ingestion includes Staff et al. (2016), requiring a giant star, Bear, Kashi & Soker (2005), with a brown dwarf primary and timescales of only a few days for the brightening, much less than observed in the 1670s, and Siess & Livio (1999) finding a maximum amplitude less than 1000, and brightening extending over $\sim 10^4$ yr. None of these are consistent with the luminosity or timescales present in CK Vul. Thus we exclude planet ingestion by stars in the range from brown dwarfs to giants.

4.3 White Dwarf merger with a Brown Dwarf

While a stellar merger has been the favoured interpretation for CK Vul (Kamiński et al. 2017) it seems that no primary star with an intact envelope prior to 1670 can evolve in a manner consistent with the observed characteristics of CK Vul. We turn to the results in Section 3 to explore an alternative model.

While the nature of CK Vul prior to 1670 is currently unknown, it is indisputable that the morphology and extent of the associated nebula is similar to other objects including asymmetric planetary nebulae (APN). The shaping of these objects has been progressively demonstrated to be due to jet outflows generated following the formation of the nebula through the ejection of the stellar envelope. Sahai et al. (1998) proposed that dust cocoons in CRL 2688 were formed by jets expanding out into the surrounding nebulosity. Subsequent work has found that jets in APN originate with a disc around a companion to the central star (e.g. Akashi & Soker 2017a,b; Cárdenas et al. 2017; Estrella et al. 2017; Akashi, Bear & Soker 2018). The observed alignment between the dust cocoons, the jets and the bubbles demonstrate that the explanation of APN morphology could also apply to CK Vul. We also believe the innermost structures seen with ALMA are consistent with a disc.

What then is the origin of this disc? We have already excluded the sorts of progenitors that would be necessary for a merger involving main sequence or giant stars. The common envelope phase that precedes PN formation in binary systems would have been visible prior to 1670. Thus we need an alternative origin.

We suggest that all the observed characteristics of CK Vul are consistent with a *merger between a white dwarf (WD) primary and a brown dwarf (BD) secondary*. This would result in the observed "extraordinary" (Kamiński et al. 2017) isotopic composition, as the ejecta would be the disrupted brown dwarf, subjected to nuclear burning at elevated temperatures during the merger event. The estimated ejecta mass is also consistent with that of a BD. Hajduk et al. (2007) argue that the central object must have an effective temperature in the $4 - 10 \times 10^4$ K range, consistent with a WD that has experienced recent nuclear burning in accreta at its surface. They also identify elevated levels of lithium in the ejecta, further supporting nucleosynthesis at the point of merger. Unlike other merging stellar object models (e.g. Kamiński et al. 2018), there is no barrier to prevent the products of the nucleosynthesis being ejected from

the merger event almost immediately, as this takes place on the WD surface. The BD material that is not ejected would necessarily form an accretion disc due to the orbital angular momentum. This then generates the conditions required to support the observed jets at some point after the initial ejection events in the 1670s. The jets go on to inflate the bubbles and generate the dusty cocoons observed in Figs. 3 and 2 over the subsequent centuries.

5 CONCLUSIONS

We have imaged the inner regions of the extended emission associated with CK Vul in unprecedented detail. The dust emission is found to trace a warped disc extended east–west about 1400 AU, a pair of cocoons extending $\sim 5''$ to the north and south, and two additional clouds $2''$ in extent located $6''$ to the north and south of the central peak, which coincides with free–free radio emission detected by Hajduk et al. (2007).

In addition we have imaged extended emission in at least eight lines, which are resolved at a modest level of ~ 22 km s^{-1}. This is sufficient to show a jet traced by CH_3OH and extended bubbles traced by CN, both well–aligned with the dust emission. The extension of the inner feature in the central compact structure also aligns with the jet axis. The mapped emission is consistent with a CO jet detected by Kamiński et al. (2015), as well as structures traced in numerous molecules including AlF by Kamiński et al. (2018), and it seems reasonable to assume we have resolved it. Some lines detected are consistent with bubbles seen in CN, with other molecules tracing the jet. The S–shape of the jet is consistent with precession at an unknown period. Further dynamic modelling of these lines will allow us to better understand the interactions between these components; this work will be presented elsewhere.

We make comparisons with the predictions of two stellar–merger models, and note that many of the features seen in Nova Vul 1670 are consistent with such an origin. However in general the invisibility of the central star prior to 1670 is inconsistent with any stellar merger scenario for main sequence or giant stars, in line with the conclusions of Evans et al. (2016). We also exclude planet ingestion as this cannot explain the duration of the brightening events in the 1670s.

We suggest instead that Nova Vul 1670 was due to the merger of a white dwarf and a brown dwarf. This is consistent with our mass determination for the nebula imaged with ALMA and in Hα. Jets forming dust cocoons and cavities, as seen in CK Vul, are believed to cause similar structures in APN. We argue that the brown dwarf impact generates the unusual abundances and isotopic ratios seen in this object via nucleosynthesis, then forms the extended ejecta and disc observed with ALMA and that in turn drives the jets shaping the inner $\sim 6''$ north and south of the centre of the jet and disc. This would include generating and distributing the ^{26}Al recently imaged by Kamiński et al. (2018).

ACKNOWLEDGEMENTS

REFERENCES

Akashi M., Bear E., Soker N., 2018, MNRAS, 475, 4794

Akashi M., Soker N., 2017a, IAUS, 323, 227

Akashi M., Soker N., 2017b, MNRAS, 469, 3296

Baars J.W. M., Hooghoudt B. G., Mezger P. G., de Jonge M. J., 1987, A&A, 175, 319

Bally J., Zinnecker H., 2005, AJ, 129 2281

Bear E., Kashi A., Soker N., 2011, MNRAS, 416, 1965

Carlberg J. K., Cunha K., Smith V. V., Majewski S. R., 2012, ApJ, 757, 109

Cárdenas M. W. B., Vázquez R., Kaeufl H. U., Gómez-Muñoz M. A., Guillén P. F., Guerrero M. A., Miranda L. F., 2017, IAUS, 323, 363

Currie M.J., Berry D. S., Jenness T., Gibb A. G., Bell G. S., Draper P. W., 2014, in Astronomical Data Analysis Software and Systems XXIII. eds N. Manset, P. Forshay, Astronomical Society of the Pacific

de Marco O., 2009, PASP, 121, 316

Estrella D., Hernández-Martínez L., Velázquez P. F., Esquivel A., Raga C. A., 2017, IAUS, 323, 373

Evans A., van Loon J. Th., Zijlstra A. A., Pollacco D., Smalley B., Tyne V. H., Eyres S. P. S., 2002, MNRAS, 332, L35

Evans A., et al., 2016, MNRAS, 457, 2871

Ginzburg S., Sari R.,2017, MNRAS, 469, 278

Gómez L., Rodríguez L. F., Loinard L., Liziano S., 2005, ApJ, 635, 1166

Güsten R., et al., 2004, Proc. SPIE, 6267, 626714

Hajduk M., et al., 2005, Science, 308, 231

Hajduk M., et al., 2007, MNRAS, 378, 1298

Hajduk M., van Hoof P. A. M., Zijlstra A. A., 2013, MNRAS, 432, 167

Ho P. T. P., Moran J. M., Lo K. Y., 2002, ApJ, 616, L1

Kamiński T., Menten K. M., Tylenda R., Hajduk M., Patel N. A., Kraus A., 2015, Nature, 520, 322

Kamiński T., Menten K. M. , Tylenda R., Karakas, A. Belloche A., Patel N. A., 2017, A&A, 607, A78

Kamiński T., Tylenda R., Menten K. M., et al. 2018, arXiv:1807.10647

Kato T., 2003, A&A, 399, 695

MacLeod M., Cantiello M., Soares-Furtado M., 2018, ApJ, 853, L1

Maeder A., 2009, Physics, Formation and Evolution of Rotating Stars, Chapter 2, Astronomy and Astrophysics Library, Springer Berlin, Heidelberg

Massarotti A., Latham D. W., Stefanik, R. P., Fogel J., 2008, AJ, 135, 209

McMullin, J. P., Waters, B., Schiebel, D., Young, W., Golap, K., 2007, Astronomical Data Analysis Software and Systems XVI (ASP Conf. Ser. 376), ed. R. A. Shaw, F. Hill, & D. J. Bell (San Francisco, CA: ASP), 127

Mennella, V., Colangeli, L., Bussoletti, E., 1995, A&A, 295, 165

Metzger, B. D., Pejcha, O., 2017, MNRAS, 471, 3200

Nixon C. J., Pringle J. E., 2010, MNRAS, 403, 1887

Otsuka M., Parthasarathy M., Tajitsu A., Hubrig S., 2017, ApJ, 838, 71O

Pratchett T., 2013, Raising Steam, Doubleday

Privitera G., Meynet G., Eggenberger P., Vidotto A. A. Villaver E., Bianda M., 2016, A&A, 593, A128

Retter A., Marom A., 2003. MNRAS, 345, L25

Retter A., Zhang B., Siess L., Levinson A., 2006, MNRAS, 370, 1573

Rushton M. T., Geballe T. R., Filippenko A. V., Chornock R., Li W., Leonard D. C., Foley R. J., Evans A., Smalley B., van Loon J. Th., Eyres S. P. S., 2005, MNRAS, 360, 1281

Sahai R., Trauger J. T., Watson A. M., Stapelfeldt K. R. and Hester J. J., Burrows C. J., Ballister G. E. and Clarke J. T., Crisp D., Evans R. W., Gallagher III, J. S. and Griffiths R. E., Hoessel J. G., Holtzman J. A. and Mould J. R., Scowen P. A., Westphal J. A., 1998, ApJ, 493, 301

Sarkar G., Sahai R., 2006, ApJ, 644 1171

Shara M. M., Moffat A. F. J., 1982, ApJ, 258, L41

Shara M. M., Moffat A. F. J., Webbink R. F., 1985, ApJ, 294, 271

Siess L., Livio M., 1999, MNRAS, 308, 1133

Soker N., Tylenda R., 2007, ASP Conference Series, 363, 280

Staff J. E., De Marco O., Wood P., Galaviz P., Passy J.-C., 2016, MNRAS, 458, 832

van Kempen T. A., et al., 2015, ALMA Memo 599, NRAO Library

Wallace P. T., Clayton C. A., 1997, Starlink User Note 78.9

Walsh J. R., Monreal-Ibero A., Barlow M. J., Ueta T., Wesson R., Zijlstra A. A., 2016, A&A, 588, A106

Walsh C., Daley C., Facchini S., Juhász A., 2017, A&A, 607, 114

Wootten A., Thompson A. R., 2009, Proc. IEEE, 97, 8, 1463

This paper has been typeset from a TeX/ LaTeX file prepared by the author.